



Transport of *Pseudomonas aeruginosa* in Polymer Solutions

Giovanni Savorana¹, Steffen Geisel², Tianyu Cen¹, Yuya Ling¹, Roman Stocker¹, Roberto Rusconi^{3,4} and Eleonora Secchi^{1*}

¹Institute of Environmental Engineering, Department of Civil, Environmental and Geomatic Engineering, ETH Zurich, Zurich, Switzerland, ²Laboratory for Soft Materials, Department of Materials, ETH Zurich, Zurich, Switzerland, ³Department of Biomedical Sciences, Humanitas University, Pieve Emanuele, Italy, ⁴IRCCS Humanitas Research Hospital, Rozzano, Italy

Bacteria often live surrounded by polymer solutions, such as in animal respiratory, gastrointestinal, and reproductive tracts. In these systems, polymer solutions are often exposed to fluid flow, and their complex rheology can affect the transport of chemical compounds and microorganisms. Recent studies have focused on the effect of polymer solutions on the motility of bacteria in the absence of fluid flow. However, flow can be a game-changer on bacterial transport, as demonstrated by the depletion of motile bacteria from the low-shear regions and trapping in the high-shear regions in simple fluids, even for flows as simple as the Poiseuille one. Despite the relevance of polymer solutions in many bacterial habitats, the effect of their complex rheology on shear-induced trapping and bacterial transport in flow has remained unexplored. Using microfluidic experiments and numerical modeling, we studied how the shear rate and the rheological behavior of Newtonian and non-Newtonian polymer solutions affect the transport of motile, wild-type *Pseudomonas aeruginosa* in a Poiseuille flow. Our results show that, in Newtonian solutions, an increase in viscosity reduces bacterial depletion in the low-shear regions at the microchannel center, due to a reduction in the bacterial swimming velocity. Conversely, in the non-Newtonian solution, we observed a depletion comparable to the buffer case, despite its zero-shear viscosity being two orders of magnitude higher. In both cases, bacterial swimming and polymer fluid rheology control the magnitude of bacterial depletion and its shear-rate dependence. Our observations underscore the importance of the rheological behavior of the carrier fluid in controlling bacterial transport, in particular, close to surfaces giving rise to velocity gradients, with potential consequences on surface colonization and biofilm formation in many naturally relevant microbial habitats.

Keywords: bacterial motility, poiseuille flow, polymer solution, microfluidics, rheology, *Pseudomonas aeruginosa*

INTRODUCTION

Polymer fluids are found in the natural habitat of bacteria, as in organs covered in mucus [1], or in technological settings, like groundwater remediation and enhanced oil recovery [2]. In these systems, polymer fluids are often in flow, and their polymeric nature determines their complex rheology, which in turn affects the transport of chemicals, particles and microorganisms. Complex rheological behaviors include viscoelasticity, shear-thinning, and shear-thickening, where viscosity gradients can arise in the presence of shear rate gradients [3].

OPEN ACCESS

Edited by:

Xiang Cheng,
University of Minnesota Twin Cities,
United States

Reviewed by:

Bin Liu,
University of California, Merced,
United States
Harold Auradou,
Fluides, Automatique et Systèmes
Thermiques (FAST), France

*Correspondence:

Eleonora Secchi
esecchi@ethz.ch

Specialty section:

This article was submitted to
Biophysics,
a section of the journal
Frontiers in Physics

Received: 01 April 2022

Accepted: 31 May 2022

Published: 30 June 2022

Citation:

Savorana G, Geisel S, Cen T, Ling Y,
Stocker R, Rusconi R and Secchi E
(2022) Transport of *Pseudomonas*
aeruginosa in Polymer Solutions.
Front. Phys. 10:910882.
doi: 10.3389/fphy.2022.910882

In no-flow conditions, polymer solutions affect bacterial swimming because of their complex rheology. Pioneering work of the 70' reported that a moderate increase in the viscosity of the suspending medium causes an increase in the swimming velocity of several species of flagellated bacteria, whereas a further increase in viscosity reduces it [4–7]. This observation was first explained in terms of gain in propulsive efficiency of the flagellum at moderate viscosities [4, 8]. Lately, the characteristics of the polymer network were also evaluated: experimental observation and a mathematical model have shown that the hydrodynamic forces exerted by the polymer network on the swimming cell body are responsible for the change in the bacterial swimming [5, 9]. This explained the observed dependence of the swimming velocity not only on the viscosity, but also on the type of polymer. Recent research studies further described how the local shear-thinning [10, 11], the elastic properties of the polymer solution [11–14] and the hydrodynamic interaction between individual bacteria and the colloidal component of complex fluids [15] are responsible for the change in swimming pattern and velocity of bacteria. Additionally, the influence of the details of the bacterial swimming behavior is currently under investigation [16–19]. The complexity of polymer rheology, the diversity of the bacterial propulsion strategies, and their interplay hindered the development of a unified description of swimming in polymer solutions. However, the key ingredients at play when the fluid is at rest have been identified.

Conversely, bacterial transport by flowing polymer solutions remains understudied. Water flow has been shown to affect bacterial transport and distribution, as described in several studies [20–22]. In a straight microfluidic channel, motile bacteria become trapped close to flat surfaces, causing their accumulation in the proximity of the channel walls and depletion from the central region of the channel [23]. This trapping is a hydrodynamic phenomenon determined by the action of fluid shear on motile, elongated bacteria [23–26], driving bacterial accumulation behind obstacles [27–29] and in the wake of sinking spheres [30]. These results were obtained in water, while, to date, the effect of flow of the polymer solutions has not been explored yet. In a polymer solution in flow, two elements could affect bacterial transport: the complex rheology of the fluid, potentially leading to the creation of viscosity gradients, and its effect on bacterial motility. The interplay between these two effects could completely change the observations compared to the case of water, with practical implications for the medical and industrial sectors.

In this work, we show that polymer fluids affect the transport of bacteria in a Poiseuille flow in a different way compared to the water case. By using both a Newtonian—polyvinylpyrrolidone (PVP)—and a non-Newtonian—xanthan gum—polymer solution as suspending fluids, we studied the transport of motile *Pseudomonas aeruginosa* PA14 wild-type cells in a serpentine microfluidic channel. First, we characterize the motility of the bacterial cells in the two polymer solutions at different concentrations in the absence of flow. Then, by coupling experiments and a mathematical model, in the Newtonian case, we show that increasing the polymer concentration both delays and reduces bacterial depletion from the channel center, as a

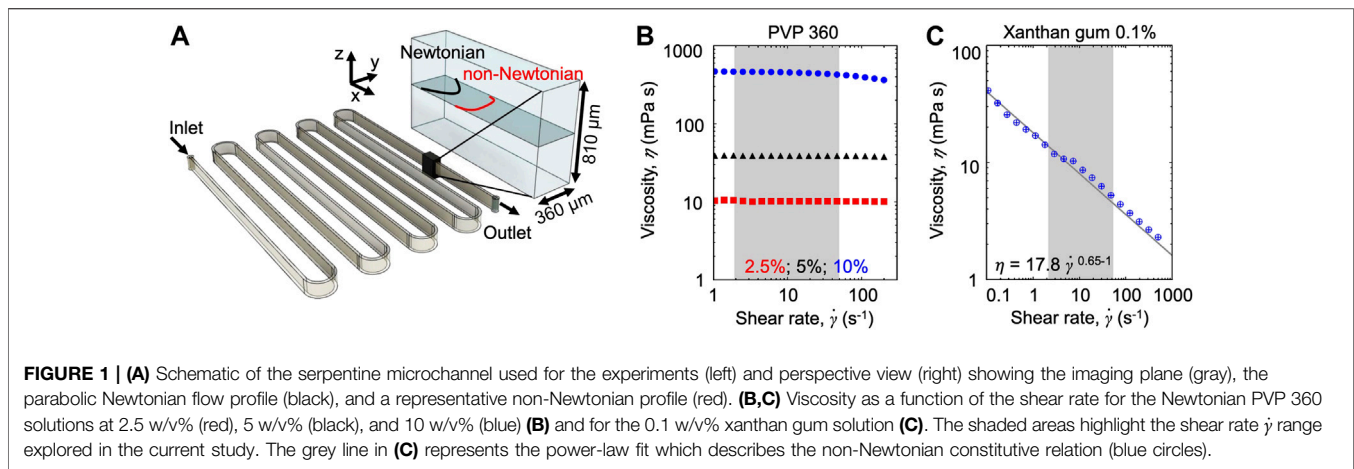
result of the reduction of the bacterial swimming velocity. In the non-Newtonian case, we show that bacterial depletion is not significantly reduced compared to the buffer case as the high zero-shear viscosity in the Newtonian case would suggest. This result is due to the high values of the swimming velocity V in the xanthan gum solution and to the non-Newtonian shear rate profile across the channel width. Taken together, these results suggest that the complex rheology of polymer solutions has a crucial impact on bacterial transport.

MATERIALS AND METHODS

Polymer solutions. Polyvinylpyrrolidone (PVP) 360 (Sigma Aldrich) powder was suspended in phosphate-buffered saline (PBS) to a concentration of 15 w/v% and stirred overnight on a magnetic stirrer at ambient temperature. The polymer solution was then diluted to the final concentrations of 2.5 w/v%, 5 w/v%, and 10 w/v% by adding PBS and a fixed volume of bacterial suspensions. Xanthan gum powder from *Xanthomonas campestris* (Sigma Aldrich) was suspended in 85 mM NaCl solution to a concentration of 0.2 w/v% and stirred for 48 h on a heated magnetic stirrer at 65°C. The xanthan gum solution was then diluted with the bacterial suspension to a final concentration of 0.1 w/v%.

Rheological characterization of the polymer solutions. The viscosity of the polymer solutions was measured using a modular compact rheometer (MCR-302, Anton Paar). We used both cone plate (CP50-2) and double gap (DG26.7) geometries to obtain the flow curve of the polymer solution at each concentration. For each measurement, the shear rate was increased from 0.1 s^{-1} to 500 s^{-1} and then decreased from 500 s^{-1} to 0.1 s^{-1} while 5 logarithmically spaced measurement points per decade were recorded for 15 s each point.

Bacterial cultures. Experiments were performed using *P. aeruginosa* strain PA14 wild type. *P. aeruginosa* suspensions were prepared by inoculating 3 ml of Tryptone Broth (TB, 10 g L⁻¹ tryptone) with cells from a frozen stock and incubating overnight at 37°C while shaking at 200 rpm. Approximately 30 μl of solution were then resuspended in 3 ml of the same medium and incubated under the same conditions for 5 h ($\text{OD}_{600} = 1$). To ensure a high percentage of motile bacteria in the experiments, non-motile and dead cells were gently removed from bacterial suspensions using sterile cell culture inserts incorporating a 3- μm -pore-size membrane, following the procedure described in [23, 29]. The filtered bacterial suspension was then mixed with the polymer solutions to the final desired polymer concentration and immediately used in the experiments. For the polymer-free control, the filtered bacterial suspension was resuspended in phosphate-buffered saline (PBS). Growth curves were acquired by measuring the OD_{600} of the bacterial suspensions in PVP 360 (2.5 w/v %, 5 w/v %, and 10 w/v %) and in xanthan gum (0.1 w/v %) solutions while incubated for 5 h at 37°C and shaking at 200 rpm. The growth curves did not show any differences from the PBS buffer case, suggesting that the bacteria did not metabolize the chosen polymers.



Microfluidic assays. We fabricated a poly-dimethyl-siloxane (PDMS) [31] microfluidic device with a single 50 cm-long serpentine channel (**Figure 1A**). The serpentine channel is composed of 13 parallel straight sections, connected by curves with an inner radius $R = 500 \mu\text{m}$. Each straight section is 4 cm long. To ensure that the dominant velocity gradients occurred on the observation plane, we designed the microchannel with aspect ratio $H/W = 2.25$ (height $H = 810 \mu\text{m}$; width $W = 360 \mu\text{m}$). Flow was driven by a syringe pump (neMESYS 290N, CETONI, Germany), at constant flow rates in the range $Q = 4.5\text{--}180 \mu\text{l min}^{-1}$. At such flow rates, the mean of the absolute value of the shear rate $|\dot{\gamma}(y)|$ on the horizontal midplane of the channel, defined as $S \equiv \frac{1}{W} \int_{-W/2}^{W/2} |\dot{\gamma}(y)| dy$, varied in the range $2.5\text{--}100 \text{ s}^{-1}$. Prior to use, all the microfluidic channels were washed with 2 ml of medium. Then, a diluted suspension of PA14 cells ($\text{OD}_{600} < 0.01$; cell concentration $< 10^6 \text{ cells ml}^{-1}$) was flown for the time required to replace the medium in the entire length of the channel (30 s–1 min, depending on the flow rate Q). The suspension was left at rest until the bacterial concentration was homogeneous. Finally, the flow was started and images were acquired at a distance of 50 cm from the inlet after a time required for the homogeneous suspension to travel 50 cm (30 s–1 min, depending on the flow rate Q). To characterize bacterial motility in polymer solutions, the same samples used for the transport experiments were loaded in 1 cm-long, $100 \mu\text{m}$ -high and 3 mm-wide PDMS chambers. The chambers were sealed to avoid drifts during the imaging. All the experiments were performed at room temperature.

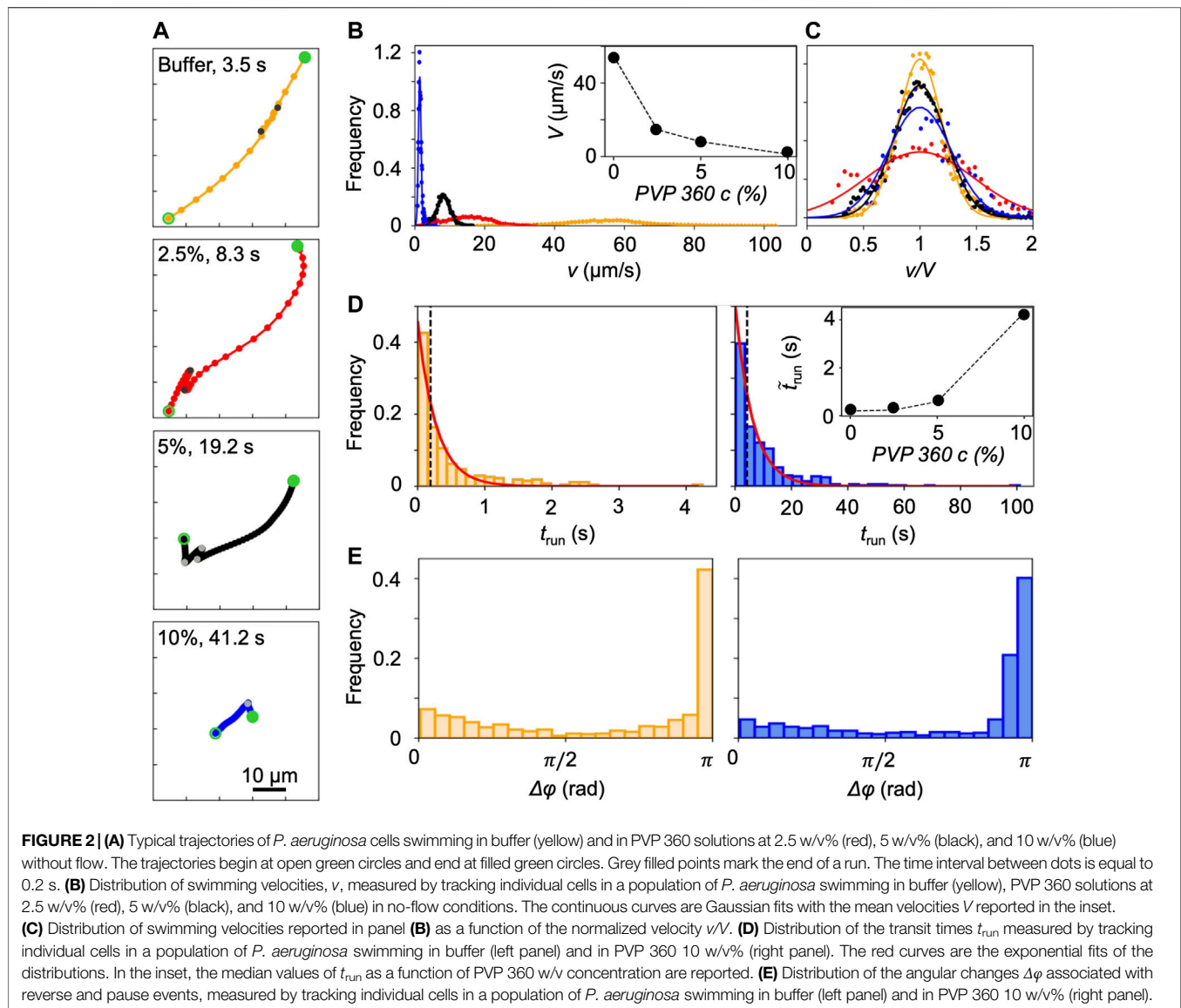
Cell imaging and tracking. All imaging was performed on an inverted microscope (Ti-Eclipse, Nikon, Japan) using a digital camera (ORCA-Flash4.0 V3 Digital CMOS camera, Hamamatsu Photonics, Japan). Bacterial trajectories for motility characterization (**Figure 2A**) were extracted from time-lapse dark-field acquisitions (15 \times magnification; 87 frames per second (fps) in buffer, 20 fps in PVP 360 2.5 w/v% solution, 10 fps in PVP 360 5 w/v% solution, 5 fps in PVP 360 10 w/v% solution); 1,300 images were acquired in each polymer solution. To quantify bacterial transport in polymer solutions, images were acquired with phase-contrast microscopy (30 \times magnification, 25 fps); 3,000 images were acquired in every experimental condition. We experimentally measured the bacterial concentration B by

counting bacterial cells in the laminar flow at a distance of 50 cm from the channel inlet. The concentration B was normalized by the initial homogeneous concentration and averaged over the imaging region, as in [23]. All image analysis was performed in Matlab (The Mathworks) using in-house cell tracking algorithms. The experiments were repeated three times with consistent results, but the data shown are from a single realization.

Numerical simulations. The mathematical model, adapted from [23], describes the transport of individual swimming bacteria by the two-dimensional (2D) velocity field inside the microchannel, for the same velocity and flow conditions used in the experiments. The equations of motion of an ellipsoidal swimmer in a 2D flow directed along the x axis are:

$$\begin{aligned} \dot{x} &= V \cos(\phi) + u(y) \\ \dot{y} &= V \sin(\phi) \\ \dot{\phi} &= -\frac{1}{2} \frac{\partial u(y)}{\partial y} \left(1 + \frac{1-q^2}{1+q^2} \cos(2\phi) \right) + \xi_R(t) \end{aligned} \quad (1)$$

where V is the bacterial swimming velocity, directed along the cell major axis, $u(y)$ is the flow speed inside the channel, ϕ is the angle between the major axis of the cell and the direction of flow, and $\xi_R(t)$ describes the angular deviations due to thermal noise and the specific bacterial swimming pattern. Here, *P. aeruginosa* cells were modeled as prolate ellipsoids with an effective aspect ratio $q = 9.4$ [29] and the swimming velocity V was set according to the values measured in our motility assays. We numerically integrated the equations of motion for 10^5 cells with a fourth-order Runge-Kutta scheme implemented in Matlab (The MathWorks) with time step $\Delta t = 4 \text{ ms}$. In order to take into account the run-reverse-pause motility of *P. aeruginosa*, we integrated the equations of motion for a number of time steps equal to $t_{\text{run}}/\Delta t$ by modeling $\xi_R(t)$ as the thermal rotational noise described by a Gaussian-distributed angular velocity with zero mean and variance $2D_{\text{rot}}/\Delta t$, where $D_{\text{rot}} = 0.0014 \text{ rad}^2/\text{s}$ is the Brownian rotational diffusion coefficient of a cell with aspect ratio $q = 9.4$ and a width of $1 \mu\text{m}$. After every $t_{\text{run}}/\Delta t$ steps, we modeled the reverse-pause events by adding a random angular deviation $\Delta\phi$ drawn by the angular distributions measured experimentally. The results did not change significantly when considering the



Brownian rotational diffusion coefficient of a cell without taking the flagellum into account (aspect ratio $q = 2$, $D_{\text{rot}} \approx 0.05 \text{ rad}^2/\text{s}$).

In the case of Newtonian fluids flowing in a straight channel, we considered a parabolic velocity profile $u(y) = U[1 - 4(y/W)^2]$, where U is the maximum flow speed, and a shear rate profile $\dot{\gamma}(y) = \partial u(y)/\partial y = -8Uy/W^2$. To simulate the Newtonian flow in a serpentine channel as the one used in the experiments, we first characterized the three-dimensional (3D) flow in the channel curves with computational fluid dynamics (CFD) simulations (COMSOL Multiphysics). Then, we numerically integrated Eq. 1 by alternating sections with the velocity and shear rate profiles of the 4 cm-long straight sections and sections mimicking the curves to the left or to the right, according to the channel geometry. The length of the sections mimicking the curves was set to $(R + W/2)\pi$ and the corresponding velocity and shear rate profiles were assumed to be equal to those computed on the channel midplane at the center of a curve.

In the non-Newtonian case, we first characterized the 3D flow of the 0.1 w/v% xanthan gum solution inside the microchannel with CFD simulations. We then used the resulting 2D velocity and shear rate profiles on the midplane to integrate the equations of motion in Eq. 1. To simulate the rheological behavior of the xanthan gum solution, we set the fluid consistency index to $m = 17.8 \text{ mPa}\cdot\text{s}$ and the flow behavior index to $n = 0.65$, according to our rheological measurements (Figure 1C). We set the lower shear rate limit to $\dot{\gamma}_{\text{min}} = 0.00188 \text{ s}^{-1}$. According to the shear-thinning behavior of xanthan gum solutions, channel flow gives rise to viscosity gradients. In our modelling, we do not explicitly account for any shear-thinning effect taking place at the microscale under the action of flagellar motion. In the following, we refer to the viscosity $\eta = \eta(y)$ determined only by channel flow as ambient viscosity. In no-flow conditions, ambient viscosity coincides with the zero-shear viscosity η_0 .

Given that ambient viscosity is not homogeneous across the channel width, we investigated a possible dependence of bacterial swimming velocity on position. To do so, in the equations of motion for the non-Newtonian case, we considered that the swimming velocity $V = V(y)$ can vary across the channel width W , due to local changes in η . In order to find a relation between V and η , we used the following approach. We measured the swimming velocity V as a function of the xanthan gum concentration in the range $c = 0$ (buffer)—0.5 w/v%. In this concentration range, the relation between V and c is linear:

$$V = ac + d \quad (2)$$

where $a = -4.7 \cdot 10^{-9}$ (m/s) (L/mg), $d = 33.9 \cdot 10^{-6}$ m/s and c is expressed in ppm units (Figure 6A). According to [32], we established the following relation between c and the zero-shear viscosity η_0 for xanthan gum solutions in NaCl at 50 mM:

$$\eta_0(c) = \begin{cases} \frac{0.04}{500^2} c^2 = X_1 c^2 & \text{for } c \leq c_e \\ \frac{4}{2000^{4.67}} c^{4.67} = X_2 c^{4.67} & \text{for } c > c_e \end{cases} \quad (3)$$

where $c_e = 1000$ ppm is the entanglement concentration. Using this relation, we expressed V as a function of η_0 as:

$$V(\eta_0) = \begin{cases} a \left(\frac{\eta_0}{X_1} \right)^{1/2} + d & \text{for } \eta_0 \leq \eta(c_e) \\ a \left(\frac{\eta_0}{X_2} \right)^{1/4.67} + d & \text{for } \eta_0 > \eta(c_e) \end{cases} \quad (4)$$

where $\eta(c_e) = 160$ mPa s. Under the assumption that V in flowing xanthan gum solutions varies only due to the change in η , and that the dependence of V on η is the same as the one on η_0 , we calculated V as a function of η by combining Eqs 3, 4. Since the concentration of our sample was equal to c_e and xanthan gum solutions behave as shear-thinning fluids, the viscosity of the flowing sample is $\eta \leq \eta(c_e)$. According to Eq. 4, $V(\eta_0)$ was calculated in the regime $\eta \leq \eta(c_e)$. By combining Eq. 4 with the power law relating η to $\dot{\gamma}$ (Figure 1C) and the numerical results for $\dot{\gamma}(y)$, we found the following expression for $V(y)$:

$$V(y) = \begin{cases} a^*c + d & \text{for } y: \dot{\gamma}(y) \leq \dot{\gamma}^* \\ a \left(\frac{17.8 \cdot 10^{-3} \cdot (y)^{(0.65-1)}}{X_1} \right)^{1/2} + d & \text{for } y: \dot{\gamma}(y) > \dot{\gamma}^* \end{cases} \quad (5)$$

where $\dot{\gamma}^* = 1.88 \cdot 10^{-3} \text{ s}^{-1}$ is defined as $\eta(\dot{\gamma}^*) = \eta_0(c_e)$ and the behavior for $\dot{\gamma}(y) \leq \dot{\gamma}^*$ is fixed under the assumption that the swimming velocity cannot become smaller than the one measured in the no-flow case, where $\dot{\gamma} = 0$. As reported above, the lower shear rate limit used in the COMSOL simulations was set to $\dot{\gamma}^*$, since, under the aforementioned assumptions, variations of $\dot{\gamma}$ below this value did not affect the bacterial swimming velocity.

According to [23], we quantified the shear-induced depletion of both the experimental and numerical concentration profiles B with the depletion index I_D , defined as the fraction of bacteria depleted from the central half-width of the channel:

$$I_D = 2 \left(\frac{1}{2} - \int_{-0.25}^{0.25} B(\tilde{y}) d\tilde{y} \right) \quad (6)$$

Where $\tilde{y} = y/W \in [-0.5, 0.5]$ is the spanwise coordinate normalized by the channel width W .

RESULTS

Coupling Microfluidics and a Mathematical Model to Investigate *P. aeruginosa* Transport in Polymer Solutions

The effect of the polymeric nature of the fluid on bacterial transport was explored by combining microfluidic experiments with a mathematical model. During the experiments, we used optical microscopy to image the bacterial cells transported by the flow generated in a serpentine microfluidic channel (Figure 1A). The similarity of the geometry with the one presented in [23] allowed to easily compare the results. The aspect ratio of the channel $H/W > 1$ (height $H = 810 \mu\text{m}$; width $W = 360 \mu\text{m}$) ensures that the dominant velocity gradient occurred in the horizontal observation plane at the channel mid-depth. In this plane, for a Newtonian fluid—as culture media and the PVP 360 solutions—the flow profile is parabolic (Figures 1A,B), while for a non-Newtonian shear-thinning fluid—as the xanthan gum solution—the flow profile is flatter in the middle and decays faster towards the walls (Figures 1A,C). Motile *P. aeruginosa* cells were transported by the flow and imaged using video microscopy in phase-contrast mode to quantify their distribution across the width of the channel at 50 cm from the channel inlet (i.e., the entire length of the channel). Due to the low image quality close to the lateral channel walls, the cell distribution B , was quantified in a $220 \mu\text{m}$ -wide region centered at the centerline of the channel ($y/W \in [-0.3, 0.3]$).

We investigated the role of fluid rheology by comparing the results obtained with three different carrier fluids: PBS buffer, PVP 360 at different concentrations, and a 0.1 w/v% xanthan gum solution. PBS buffer had the same viscosity as water and was used as a reference fluid, as in [23]. PVP 360 solutions at different polymer concentrations were used as the prototype of the polymeric Newtonian fluid and allowed exploring the effect of a homogeneous increasing viscosity on bacterial transport (Figure 1B). The xanthan gum solution is a non-Newtonian fluid with a zero-shear viscosity $\eta_0 = 160$ mPa s, between those of PVP 360 5 w/v% and 10 w/v% and a marked shear-thinning behavior in the shear rate range explored in this study (Figure 1C). The shear-thinning behavior implies that η depends both on the flow rate and on the position y across the channel, and the shear rate profiles deviate from the linear ones observed in the Poiseuille flow of Newtonian fluids. The

Newtonian and non-Newtonian cases will be presented and analyzed individually in the following.

We observed that the polymeric nature of the carrier fluid modifies the shape of the cell distribution B and the magnitude of the depletion from the center of the channel and the accumulation towards the channel walls with respect to the buffer case. To interpret these observations, we adapted the mathematical model of cell motility in flow presented in [23, 29]. *P. aeruginosa* cells were modeled as prolate ellipsoids with aspect ratio $q = 9.4$ and swimming velocity V directed along their major axes [29]. In the Newtonian cases (buffer and PVP 360), we described the flow with a parabolic profile. In the non-Newtonian case, we characterized the flow field on the midplane of the channel with CFD simulations. The corresponding velocity and shear rate profiles were then used to compute single-cell trajectories. In both cases, the bacterial swimming direction was determined by a torque balance that accounts for the flow shear and the fluctuations in the bacterial orientation. Since the model accounts for the bacterial swimming strategy, which has been reported to change in polymeric fluids [10, 12], we characterized *P. aeruginosa* motility by tracking individual cells in the absence of flow and inserted the parameters into the model, as described in the following sub-section.

Newtonian PVP 360 Affects *P. aeruginosa* Motility in Quiescent Conditions

P. aeruginosa swims in a 3-step pattern of run-reverse-pause in buffer and PVP 360 polymer solutions at all the tested concentrations. Swimming in buffer has been described in [33, 34], in agreement with our observations. We imaged free-swimming cells on the midplane of a 100- μm high microfluidic channel, where cell motion was not affected by hydrodynamic interactions with the top and bottom walls. *P. aeruginosa* propels forward when its single polar flagellum rotates clockwise and backward when it rotates counterclockwise. Forward and backward runs are nearly straight [35] and are interrupted by pauses, sudden decreases in swimming velocity associated with small angular changes $\Delta\phi$ in the swimming direction, or reverses, associated with angular changes $\Delta\phi$ of about π [33] (yellow trajectory in **Figure 2A**). The same swimming pattern was observed in PVP 360 polymer solutions: the trajectories displayed straight runs, pauses and reverses at all the concentrations, as shown by the representative trajectories reported in **Figure 2A**. This observation indicated that the addition of PVP360 did not affect the swimming pattern of *P. aeruginosa*.

Conversely, the concentration of PVP 360 affected the distribution of swimming velocities v , measured by tracking individual *P. aeruginosa* cells. An increase in the polymer concentration led to a shift of the distribution towards lower values of v (**Figure 2B**). The distributions were fitted with Gaussian curves to estimate the mean swimming velocities V (**Figure 2B**, inset). Furthermore, the distributions of v normalized by the corresponding values of V , showed that the addition of PVP 360 caused a slight widening of the distributions, but did not affect their Gaussian shape. The widening was more

pronounced at the lowest polymer concentration (2.5 w/v%) (**Figure 2C**).

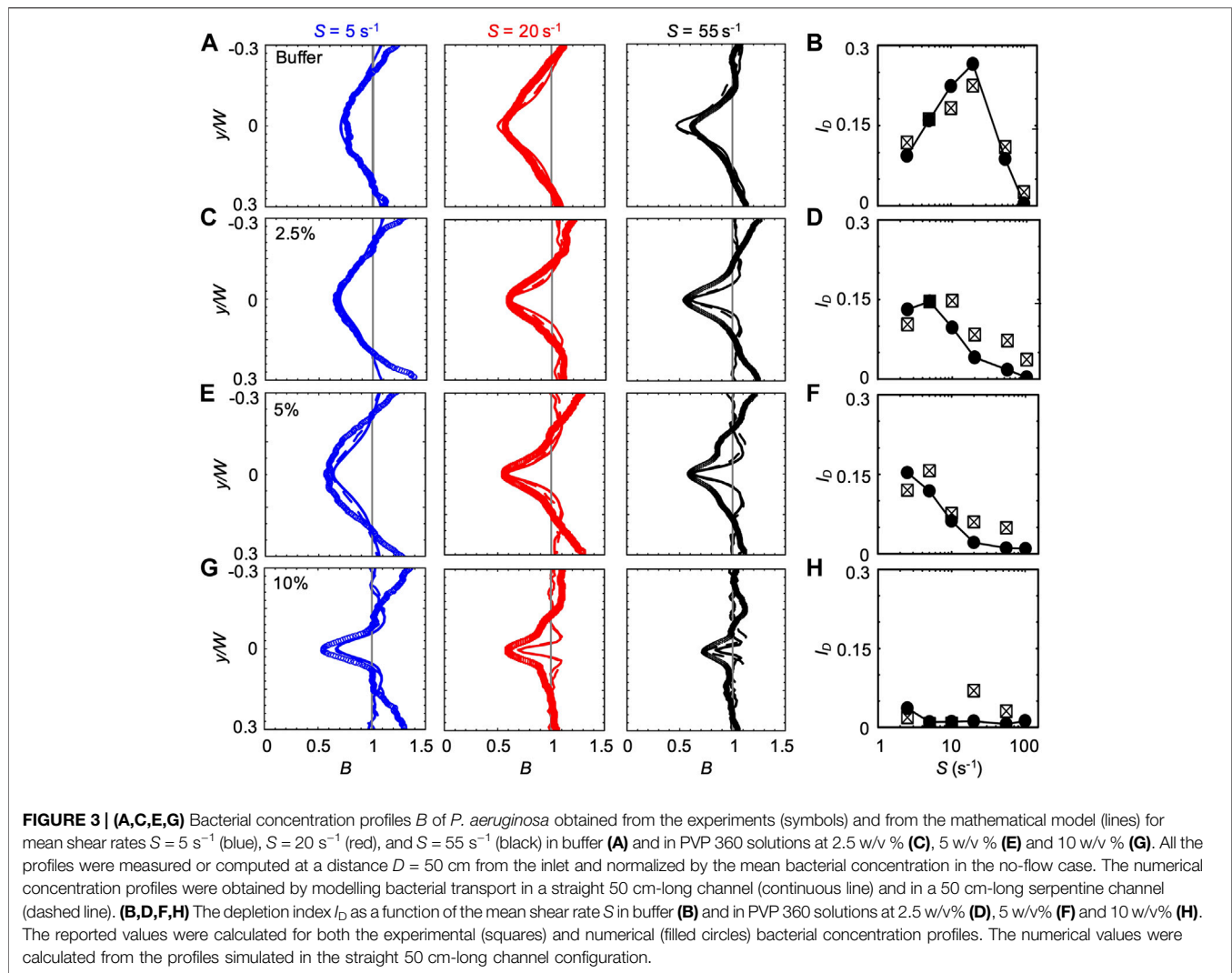
The concentration of PVP 360 also affected the distribution of transit times t_{run} (**Figure 2D**), defined as the time elapsed between two consecutive changes in direction (marked by grey points in **Figure 2A**). As in [33], t_{run} followed exponential distributions both in the buffer and in the PVP 360 solutions (red curves in **Figure 2D**). However, the median value of t_{run} increased with increasing polymer concentration (**Figure 2D**, inset). Conversely, the distribution of angular changes $\Delta\phi$ associated with pauses and reverses was not affected by PVP 360, and showed a peak at π at all the concentrations that we investigated (**Figure 2E**).

Newtonian PVP 360 Affects *P. aeruginosa* Transport in Flow

The bacterial population flowing in the channel was depleted from the center, where the shear rate $\dot{\gamma}$ was low, and accumulated in the lateral regions, where $\dot{\gamma}$ was higher, both in the buffer and in the PVP 360 polymer solutions. However, the distribution of bacterial cells across the channel width and the magnitude of the depletion effect depended on PVP 360 concentration. In the mathematical model, the bacterial motility at the different concentrations was described using the average swimming velocities V and the median values of t_{run} , reported in the insets of **Figures 2B,D**, and the distribution of $\Delta\phi$ measured in buffer (left panel in **Figure 2E**). The model allowed comparing the effect of the propagation for 50 cm in a straight channel (continuous lines in **Figure 3**) and in a serpentine channel as the one we used in the experiments (dashed lines in **Figure 3**). In buffer, our observations are consistent with [23]: for average shear rates S in the range 2.5–100 s^{-1} , the depletion increases until $S \approx 20 \text{ s}^{-1}$, and then decreases for larger shear rates.

The bacterial concentration profiles B obtained from the experiments (**Figure 3A**, symbols) were in good agreement with the ones simulated according to the mathematical model (lines) at all the tested values of S , especially when the curves in the serpentine geometry were taken into account (dashed lines). According to our simulations, the overall impact of the curves connecting the straight sections is to slightly widen the depleted region with respect to the straight channel case (dashed lines in **Figure 3**). The minimum of $|y|$ in the curves is not on the centerline, but is slightly shifted towards the center of curvature ($y > 0$ when turning to the left and $y < 0$ when turning to the right). As a consequence, when flowing in a curve, bacterial cells are more efficiently depleted in regions at the side of the centerline, causing a slight widening of the depleted region.

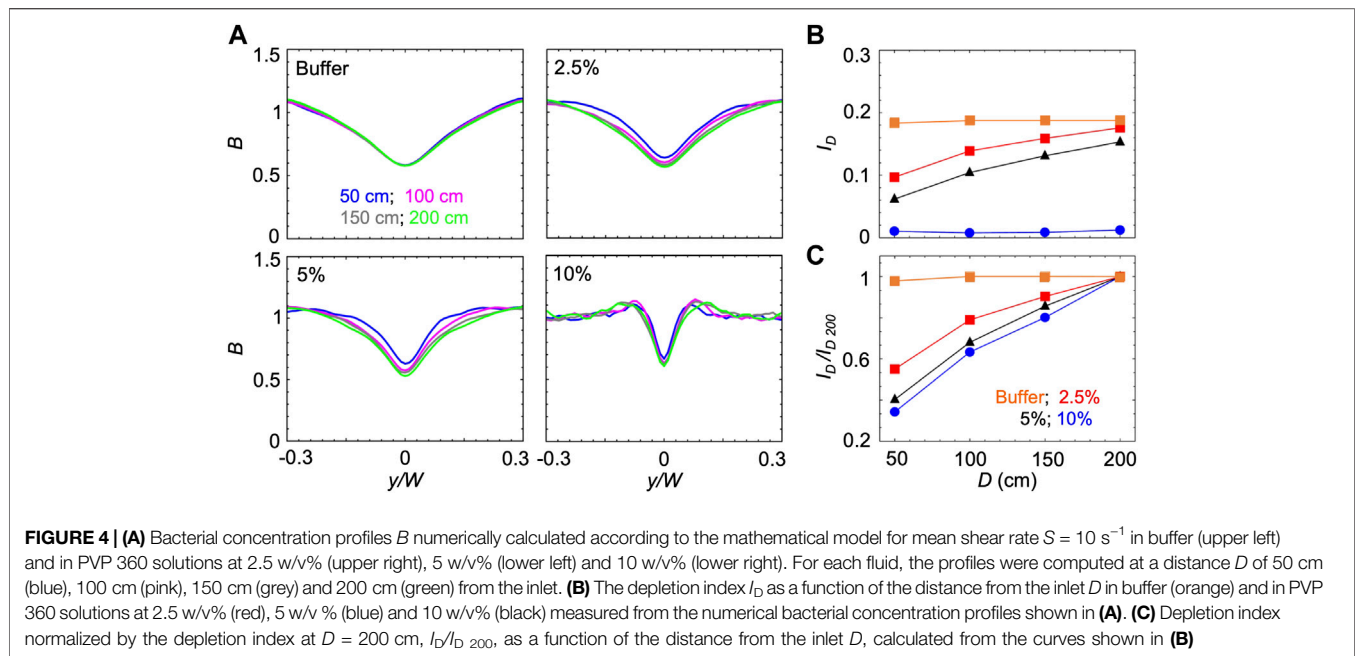
We quantified the shear-induced depletion with the depletion index I_D **Eq. 6**. The values of I_D confirm the agreement between experiments and simulations (**Figure 3B**). In the PVP 360 polymer solutions at 2.5 w/v% and 5 w/v%, the good agreement between numerical and experimental B profiles was remarkable at low S (lower than $S \approx 20 \text{ s}^{-1}$) and becomes less precise for higher values of S (**Figures 3C,E**), as confirmed by I_D (**Figures 3D,F**). Interestingly, the maximum of I_D shifted to a lower shear rate for increasing polymer concentrations ($S \approx 10 \text{ s}^{-1}$



and $S \approx 2.5 \text{ s}^{-1}$ at PVP 360 2.5 w/v% and 5 w/v%, respectively) (Figures 3D,F). The peak value of I_D was comparable at these two concentrations ($I_D \approx 0.146$ and $I_D \approx 0.153$ at PVP 360 2.5 w/v% and 5 w/v%, respectively), and was about 20% lower than the peak value of I_D in the buffer ($I_D \approx 0.19$). At the highest polymer concentration that we tested (PVP 360 10 w/v%), the agreement between the numerical and the experimental B profiles was good only for $S \leq 5 \text{ s}^{-1}$ (blue curves in Figure 3G), while for higher values of S the depletion from the center of the channel was larger in the experiments than in the model (red and black curves in Figure 3G). Additionally, I_D showed a drop in the depletion at PVP 360 10 w/v% compared to the lower polymer concentrations and the buffer case ($0.006 < I_D < 0.012$) (Figure 3H). Despite its low value, I_D decreased with increasing S , confirming the shift of the peak value of I_D to lower S values observed in PVP 360 2.5 w/v% and 5 w/v%. The transport experiments performed with dead cells (fixed by adding formaldehyde to a final concentration of 0.2%) did not show depletion at any of the PVP 360 concentrations and

values of S we tested. Overall, we observed that PVP 360 caused a decrease of the shear-induced bacterial depletion compared to the buffer case and that the decrease was higher at larger PVP 360 concentrations.

B and I_D reach steady-state values once the cells have had time to swim towards high shear regions while being transported by the flow. Thus, the time required to reach the steady state increases when the swimming velocity V decreases. Accordingly, when V decreases, the steady state distribution will be observed at larger distances from the channel inlet. Consequently, increasing the concentration of PVP 360 increased the distance required to reach the steady-state, as shown by using the mathematical model to calculate I_D as a function of the distance D from the inlet for the different solutions at $S \approx 10 \text{ s}^{-1}$ (Figure 4). In buffer, *P. aeruginosa* cells swam at $V = 54.7 \mu\text{m/s}$ and reached the steady-state distributions in less than 50 cm; thus, a longer traveling distance did not change B and I_D (Figures 4A,B). In PVP 360 solutions, B computed at a distance $D = 50 \text{ cm}$ (blue curves



in **Figure 4A**) had not reached the steady state yet, and the minima decreased when simulated at larger distances (pink and grey curves in **Figure 4A**). B reached the steady-state after 200 cm at all the tested concentrations (green curves in **Figure 4A**). The increase in the depletion with the traveling distance D was also visible from the trend of I_D (**Figure 4B**). To ease the comparison between different concentrations, we normalized I_D by its value at 200 cm, $I_D/I_{D,200}$. The normalized curves for $I_D/I_{D,200}$ showed that at higher PVP 360 concentrations the traveling distance required to reach the steady state is larger (**Figure 4C**). Consequently, we point out that in **Figure 3** we were not comparing the steady-state values for all the conditions, but the depletion reached by the bacterial suspension after flowing for 50 cm in the same channel.

The changes in the concentration profiles B and in the magnitude of the depletion observed in the PVP 360 solutions are attributable to changes in average swimming velocity V and median values of the transit time t_{run} , as shown by the good agreement between experimental and numerical results. Interestingly, if t_{run} remained constant with increasing polymer concentration, we would not observe any depletion in the 10 w/v% solution at $D = 50 \text{ cm}$. These observations suggest that an accurate description of the bacterial swimming is fundamental to accurately predict the shear-induced depletion. Consequently, in the results presented so far, we modeled the *P. aeruginosa* run-reverse-pause swimming pattern (Materials and Methods). When compared to the run-tumble pattern used to describe the motility of *B. subtilis* in [23], the run-reverse-pause motility in buffer had the same peak values, but different shapes of the depletion profile B at high shear rates (**Figure 5A**). In PVP 360 5 w/v% flowing at low S , also the peak values were different (**Figure 5C**). In the case of the buffer, a greater similarity between the B profiles simulated with run-reverse-pause and run-tumble

motility was found at the lower S , while in the case of PVP 360 5 w/v% a greater similarity was found at higher values of S . Conversely, 10% variations in the swimming velocity would not affect the depletion at any shear rate, both in the buffer and in PVP 360 (**Figures 5B,D**).

Non-Newtonian Xanthan Gum Solution Affects *P. aeruginosa* Motility and Transport

In the non-Newtonian case, the complexity of the bacterial transport is increased by the complex rheological behavior of the carrier fluid. First, due to the shear-thinning behavior of the carrier fluid, the shear rate $\dot{\gamma}$ is not linear across the channel width, as shown by CFD simulations (**Figure 7A**). Second, the ambient viscosity η varies across the channel as a function of $\dot{\gamma}$ (**Figures 1C, 7B**). Consequently, when transported by the ambient flow, bacteria swim through regions with different values of η . In this case, a dependence of V on the viscosity ($V = V(\eta)$) would imply a dependence of V also on the position y across the channel ($V = V(y)$). In addition, the shear-thinning action of the rotating flagella can also give rise to changes in η at the cell length scale.

We characterized the bacterial swimming in xanthan gum solutions at different concentrations, in no-flow conditions. By imaging free-swimming *P. aeruginosa* cells on the midplane of a 100 μm -high microfluidic channel, we observed that the non-Newtonian nature of the chosen polymer fluid did not affect the run-reverse-pause swimming pattern. As in the case of PVP 360, the average swimming velocity V decreases at increasing polymer concentration (**Figure 6A**), while the distributions of the swimming velocities v maintain a Gaussian shape (**Figure 6B**). In the case of xanthan gum, we found a linear

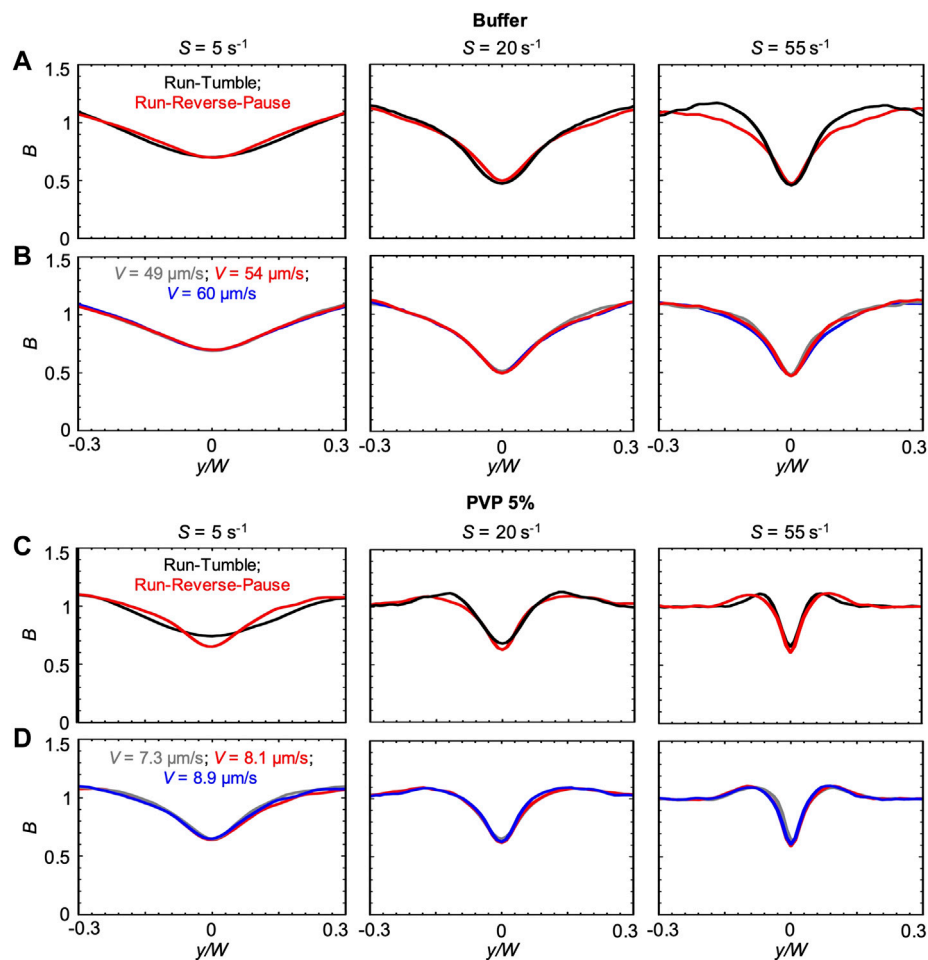


FIGURE 5 | (A) Bacterial concentration profiles B numerically calculated according to the mathematical model for mean shear rates $S = 5 \text{ s}^{-1}$ (left), $S = 20 \text{ s}^{-1}$ (center) and $S = 55 \text{ s}^{-1}$ (right) in buffer, at a distance $D = 50 \text{ cm}$ for swimmers with run-tumble (black) and run-reverse-pause (red) patterns. For the run-tumble swimmers we used $q = 9.4$, $V = 54.17 \text{ } \mu\text{m s}^{-1}$, and $D_R = 1.4 \text{ rad}^2 \text{ s}^{-1}$ as in [29], while the run-reverse-pause swimmers were simulated as described in the Materials and Methods. **(B)** Bacterial concentration profiles B calculated according to the mathematical model for mean shear rates $S = 5 \text{ s}^{-1}$ (left), $S = 20 \text{ s}^{-1}$ (center) and $S = 55 \text{ s}^{-1}$ (right) in buffer for run-reverse-pause swimmers with a swimming velocity of $V = 49 \text{ } \mu\text{m s}^{-1}$ (grey), $54.17 \text{ } \mu\text{m s}^{-1}$ (red) and $60 \text{ } \mu\text{m s}^{-1}$ (blue). **(C)** Bacterial concentration profiles B numerically calculated according to the mathematical model for mean shear rates $S = 5 \text{ s}^{-1}$ (left), $S = 20 \text{ s}^{-1}$ (center) and $S = 55 \text{ s}^{-1}$ (right) in PVP 360 5 w/v%, at a distance $D = 50 \text{ cm}$ from the inlet for swimmers with run-tumble (black) and run-reverse-pause (red) patterns. For the run-tumble swimmers we used $q = 9.4$, $V = 8.1 \text{ } \mu\text{m s}^{-1}$, and $D_R = 1.4 \text{ rad}^2 \text{ s}^{-1}$ as in [29], while the run-reverse-pause swimmers were simulated as described in the Materials and Methods. **(D)** Bacterial concentration profiles B calculated according to the mathematical model for mean shear rates $S = 5 \text{ s}^{-1}$ (left), $S = 20 \text{ s}^{-1}$ (center) and $S = 55 \text{ s}^{-1}$ (right) in PVP 360 5 w/v% for run-reverse-pause swimmers with a swimming velocity of $V = 7.3 \text{ } \mu\text{m s}^{-1}$ (grey), $8.1 \text{ } \mu\text{m s}^{-1}$ (red) and $8.9 \text{ } \mu\text{m s}^{-1}$ (blue).

relation between V and the polymer concentration c (Materials and Methods). The transit time distribution at 0.1 w/v% xanthan gum concentration followed an exponential curve as in the case of PVP 360, with a median transit time $t_{\text{run}} = 0.6 \text{ s}$. The distribution of angular changes $\Delta\varphi$ showed a peak at π (Figure 6D), as in the case of PVP 360.

The characterization of the bacterial swimming in no-flow conditions was aimed at establishing a link between the bacterial swimming parameters for the numerical model and the ambient viscosity in the channel. Ideally, it would have been advisable to characterize the swimming in a polymer solution in flow. However, this would not be possible in the presented experimental configuration. For this reason, we compared the numerical results obtained with three possible models of the

bacterial swimming in the non-Newtonian fluid in flow. In the first case, we considered a constant swimming velocity $V = V_{0.1\%}$ equal to the one measured in xanthan gum 0.1 w/v% in no-flow conditions; in the second case, we considered a dependence of the swimming velocity on the local ambient viscosity $V = V(y)$; in the third case, we considered a swimming velocity dependent on the average ambient viscosity, $V = V(\eta_s)$. Our model did not explicitly account for the flagella-induced shear thinning (Materials and Methods). However, by simulating the bacterial swimming with the parameters determined from the motility assays in xanthan gum solutions, the shear-thinning enhancement of motility in no-flow conditions is implicitly accounted for.

For the first model, we assumed that the bacterial swimming is not affected by the changes in the ambient viscosity of the carrier

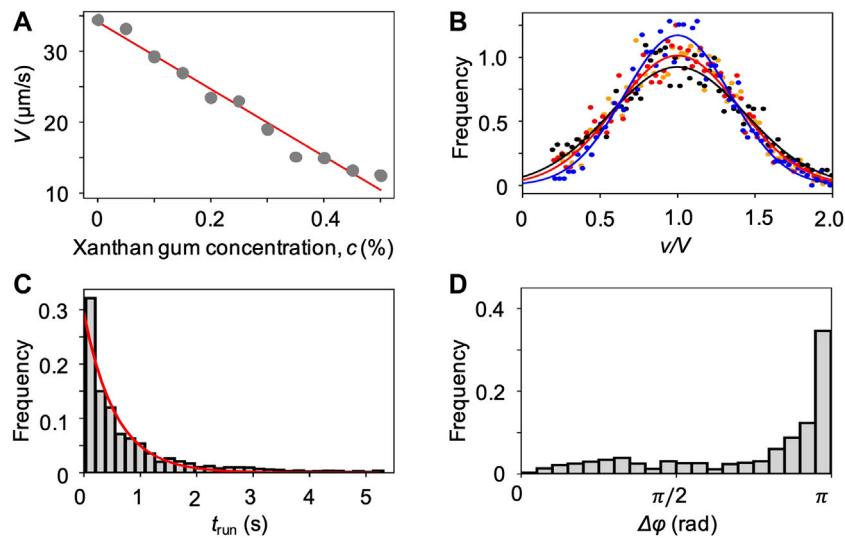


FIGURE 6 | (A) Mean swimming velocities V measured by tracking individual cells in a population of *P. aeruginosa* swimming in xanthan gum solutions at different concentrations in no-flow conditions. The red curve is the linear fit of the experimental data (Eq. 2). **(B)** Distribution of swimming velocities as a function of the normalized velocity v/V , in buffer (yellow), and in xanthan gum solutions at 0.05 w/v% (red), 0.1 w/v% (black), and 0.2 w/v% (blue) in no-flow conditions. The continuous curves are Gaussian fits with the mean velocities V reported in (A). **(C)** Distribution of the transit times t_{run} measured by tracking individual cells in a population of *P. aeruginosa* swimming in the 0.1 w/v% xanthan gum solution. The red curve is the exponential fit of the distribution. **(D)** Distribution of the angular changes $\Delta\phi$ associated with reverse and pause events, measured by tracking individual cells in a population of *P. aeruginosa* swimming in the 0.1 w/v% xanthan gum solution.

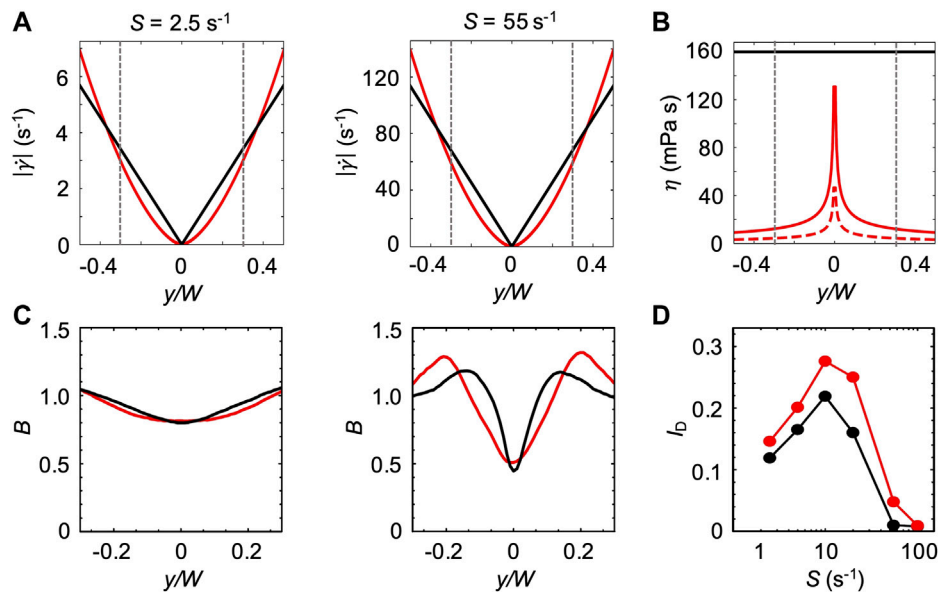
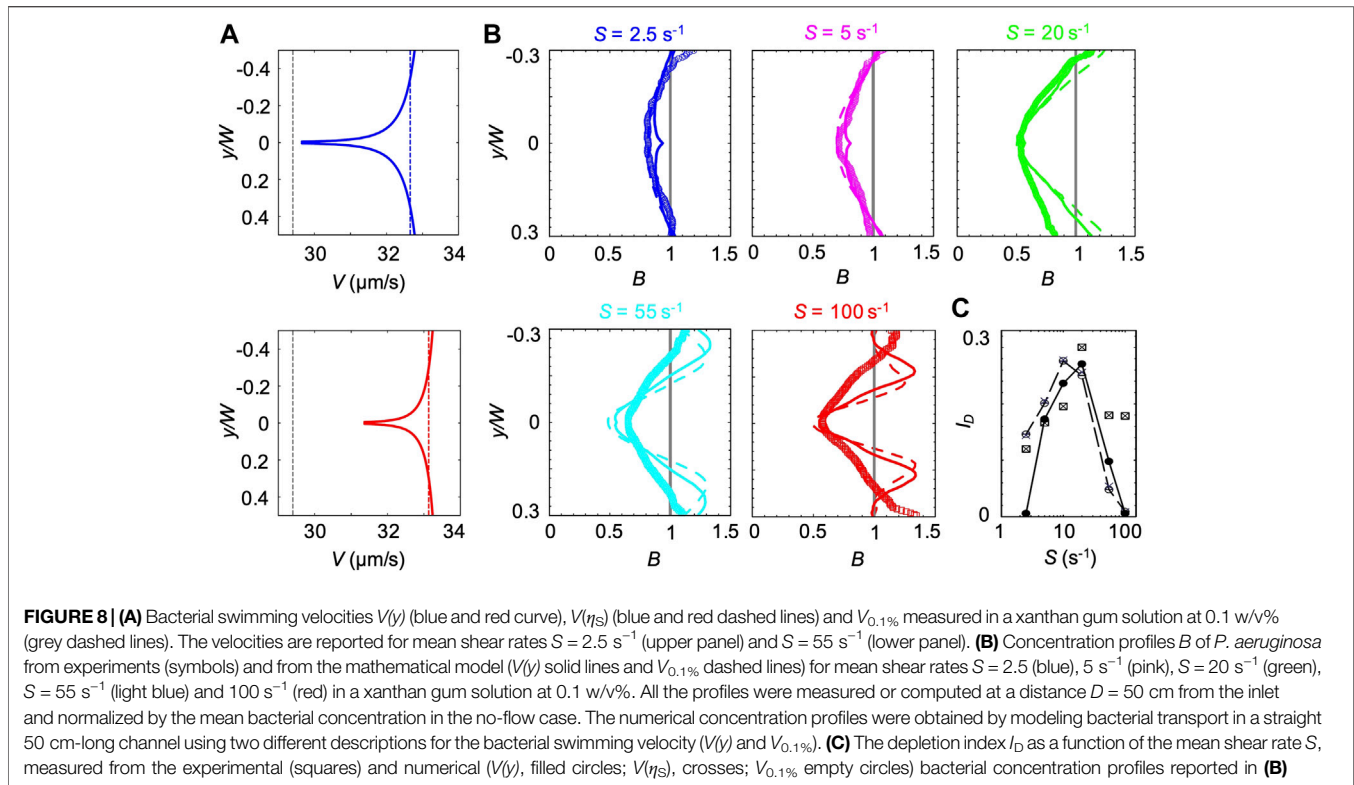


FIGURE 7 | (A) Absolute values of the shear rate $|\dot{\gamma}|$ in the channel in a Newtonian (black) and non-Newtonian (red) fluid at mean shear rates $S = 2.5 \text{ s}^{-1}$ (left panel) and $S = 55 \text{ s}^{-1}$ (right panel). The Newtonian profiles were calculated as $S = -8yU/W^2$. The non-Newtonian profiles were calculated with CFD simulations modeling the rheological behavior of xanthan gum 0.1 w/v%, as described in the Materials and Methods. **(B)** No-flow ambient viscosity η_0 of xanthan gum 0.1 w/v% (solid black line) and ambient viscosity profiles calculated with CFD simulations for $S = 2.5 \text{ s}^{-1}$ (solid red line) and $S = 55 \text{ s}^{-1}$ (dashed red line). **(C)** Concentration profiles B obtained from the mathematical model with the Newtonian (black) and non-Newtonian (red) shear rate profiles reported in panel A at mean shear rates $S = 2.5 \text{ s}^{-1}$ (left panel) and $S = 55 \text{ s}^{-1}$ (right panel). The numerical concentration profiles were obtained by modeling bacterial transport in a straight 50 cm-long channel, with bacterial swimming velocity $V = V_{0.1\%}$. **(D)** The depletion index I_D as a function of the mean shear rate S , measured from the numerical bacterial concentration calculated in the conditions described in (C).



fluid. We thus used the bacterial swimming parameters measured in xanthan gum 0.1 w/v% at rest to simulate swimming bacteria in the channel flow (**Figure 6**). In this case, the effect of the non-Newtonian behavior of xanthan gum in flow was accounted for by the shear rate profile $\dot{\gamma}$, while bacterial swimming velocity $V_{0.1\%} = 29.4 \mu\text{m/s}$, transit time t_{run} and distribution of $\Delta\phi$ were kept constant at the values measured in xanthan gum 0.1 w/v% (**Figures 7A,B**). The comparison of the concentration profiles B corresponding to the Newtonian and non-Newtonian $\dot{\gamma}$ profiles showed that cells are depleted from a wider region at the center of the channel in the non-Newtonian case, both at $S = 2.5 \text{ s}^{-1}$ and $S = 55 \text{ s}^{-1}$ (**Figure 7C**). This effect is well captured by I_D , whose peak value is 25% higher in the non-Newtonian case (**Figure 7D**). This observation indicates that the non-Newtonian shear-thinning bulk behavior of the fluid promotes cell depletion, even when its effect on the bacterial swimming behavior is not accounted for.

Since $\eta(y)$ is dependent on the position across the channel width and affects bacterial swimming (**Figures 2, 6**), in the second model, we investigated the effect of $\eta(y)$ on bacterial swimming by including a dependence of V on position. To do so, we assumed that the dependence of $V(y)$ on $\eta(y)$ is the same as the one between V and η_0 of xanthan gum solutions at different concentrations in no-flow conditions (Materials and Methods). Based on this assumption, we used the relation between V and concentration c as determined in no-flow conditions (**Figure 6; Eq. 2**), and combined it with the relation between c and η_0 (**Eq. 3**). This allowed us to express V as a function of η_0 (**Eq. 4**). According to our assumption, by assuming that $V(\eta_0)$ and $V(\eta)$ have the same functional form, we combined **Eq. 4** with the power law

describing η as a function of $\dot{\gamma}$ and obtained an expression for $V(\dot{\gamma})$. Finally, by numerically computing $\dot{\gamma}(y)$, we obtained a relation for $V(y)$ (**Eq. 5**) (blue and red solid lines in **Figure 8A**).

The third model is intermediate between the previous ones. In this case, we used the results from CFD simulations to calculate η_S , defined as the average value of $\eta(y)$ across the channel at the average shear rate S . Next, we used **Eq. 4** to compute the corresponding bacterial swimming velocity $V(\eta_S)$. $V(\eta_S)$ is constant across the channel but varies with S (blue and red dashed lines in **Figure 8A**). We then simulated the bacterial swimming using $V(\eta_S)$, and the median value of t_{run} and the distribution of $\Delta\phi$ measured in xanthan gum 0.1 w/v% in no-flow conditions.

The position-dependent swimming velocity $V(y)$ displayed a minimum at the channel centerline (red and blue solid lines in **Figure 8A**), where $|\dot{\gamma}|$ is minimum and $\eta(y)$ is maximum (**Figure 7B**). Overall, the variation of $V(y)$ across the channel width is no more than 10% of $V_{0.1\%}$. Similarly, $V(\eta_S)$ was in the range $32.5\text{--}33.2 \mu\text{m/s}$, less than 13% higher than $V_{0.1\%}$. However, the numerical results showed that the position-dependence of the bacterial swimming velocity induced a small increase in B at the centerline of the channel at $S < 55 \text{ s}^{-1}$ (blue, pink, and green solid lines in **Figure 8B**). This feature was not observed in the numerical simulations with constant bacterial swimming velocities $V_{0.1\%}$ and $V(\eta_S)$. Besides the increase at the centerline, the overall shape of B with $V(y)$ did not display any significant differences compared to the cases at $V_{0.1\%}$ and $V(\eta_S)$ (solid and dashed line in **Figure 8B**). The values of I_D obtained for the $V(y)$, $V_{0.1\%}$ and $V(\eta_S)$ cases are similar, while the

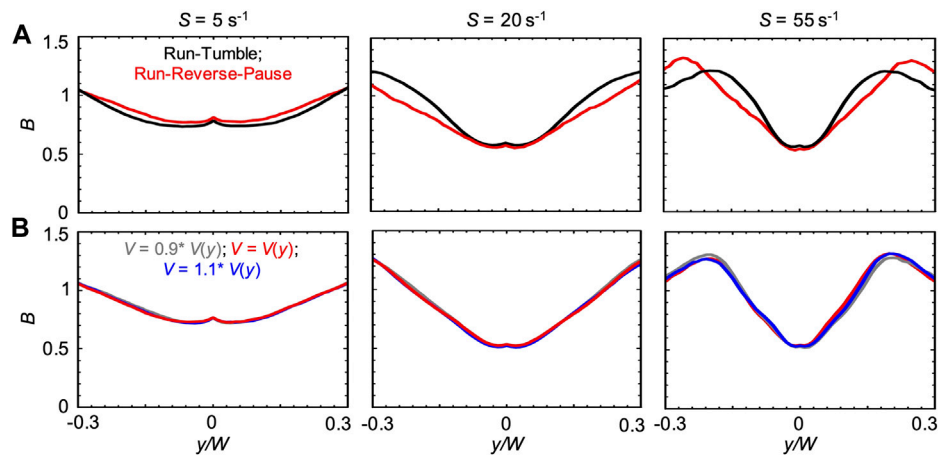


FIGURE 9 | (A) Bacterial concentration profiles B numerically calculated according to the mathematical model for mean shear rates $S = 5 \text{ s}^{-1}$ (left), $S = 20 \text{ s}^{-1}$ (center) and $S = 55 \text{ s}^{-1}$ (right) in xanthan gum 0.1 w/v %, at a distance $D = 50 \text{ cm}$ for swimmers with run-tumble (black) and run-reverse-pause (red) patterns. For the run-tumble swimmers we used $q = 9.4$, $V = 29.4 \text{ } \mu\text{ms}^{-1}$, and $D_R = 1.4 \text{ rad}^2 \text{ s}^{-1}$ as in [29], while the run-reverse-pause swimmers were simulated with swimming velocity $V(y)$, as described in the Materials and Methods. **(B)** Bacterial concentration profiles B calculated according to the mathematical model for mean shear rates $S = 5 \text{ s}^{-1}$ (left), $S = 20 \text{ s}^{-1}$ (center) and $S = 55 \text{ s}^{-1}$ (right) in xanthan gum at 0.1 w/v %, for run-reverse-pause swimmers with swimming velocities of $V(y)$, calculated according to Eq. 5 (red), $V = 0.9 V(y)$ (grey) and $V = 1.1 V(y)$ (blue).

I_D peak is shifted towards lower S in the case of constant bacterial swimming velocities $V_{0.1\%}$ and $V(\eta_S)$ (Figure 8C).

The experimental B did not display the slight increase in B at the centerline of the channel generated by the spatial dependence of $V(y)$ and showed a better agreement with the profiles obtained at constant swimming velocity (Figure 8B). However, the overall agreement between the experimental and numerical results was satisfactory at shear rates $S < 55 \text{ s}^{-1}$, as shown by B and I_D (Figures 8B,C). In this case, I_D showed a maximum at $S \approx 20 \text{ s}^{-1}$, resembling the buffer case both in the trend and the magnitude (Figure 3B).

We also compared the run-reverse-pause and run-tumble swimming patterns for the case $V(y)$. In agreement with the Newtonian case, we observed that, for run-reverse-pause swimmers, B had the same peak values but different shapes at high values of S (Figure 9A). As already suggested by the negligible differences observed in the numerical results obtained with $V_{0.1\%}$ and $V(\eta_S)$, a 10% difference in the bacterial swimming velocity did not affect B (Figure 9B). This observation is consistent with the Newtonian cases reported in Figure 6B.

DISCUSSION

How complex fluids may affect the motility of microorganisms has been the subject of several experimental [4, 10–12] and numerical [8, 11, 19] studies. On the other hand, the effect of fluid flow on bacterial transport has been investigated only in simple fluids, where a mechanistic explanation of the interplay between cell motility and hydrodynamic shear resulting in the shear-trapping of bacteria has been given [23–26, 29]. However, the influence of a polymer fluid flow on bacterial transport remained an understudied topic. Here, we focused on bacterial

transport in Newtonian and non-Newtonian polymer solutions and showed three major differences from the case of transport in water. First, the reduction of the bacterial swimming velocity V in Newtonian polymer solutions reduces bacterial depletion from the center of the channel. Second, it increases the distance D required to reach the steady-state distribution across the channel. Third, in the case of a non-Newtonian polymer solution in flow, bacterial depletion from the center of the channel is not reduced, even if the zero-shear viscosity of the fluid is much higher than the one of water. In this case, our mathematical model only captured the overall behavior of the bacterial transport. However, due to the approximations made in the model, the proposed investigation did not intend to be exhaustive. Instead, it aims at proposing a possible simplified procedure to macroscopically describe this complex problem.

The polymeric nature of the fluid plays a fundamental role in determining the motility of bacteria in no-flow conditions. In the case of *P. aeruginosa* swimming in Newtonian PVP 360 and non-Newtonian xanthan gum solutions, the swimming pattern did not change and could be described as run-reverse-pause in all the tested fluids. Similarly, the shape of the distribution of swimming velocities v and transit times t_{run} remained the same. In contrast, the mean swimming velocities V and the median of t_{run} showed significant changes, the extent of which depended on the type of polymer and its concentration in solution. In our case, the investigation in no-flow conditions was instrumental to determine the parameters describing bacterial motility to be used in the mathematical model of bacterial transport in flow.

In our study, V decreased at increasing polymer concentration, both in the Newtonian and non-Newtonian cases. Our results are consistent with recent work on *Vibrio cholerae* in PVP 360 with concentrations ranging from 0.9 to 6.7 w/w% and 1.2 w/w% mucin [7]. Conversely, previous studies performed with

Escherichia coli [10] and *P. aeruginosa* [4] in PVP 360 showed an increase in the velocity of the order of 10% at concentrations in the range between 1–2 w/v %. Considering our modelling results, a possible 10% variation in the mean swimming velocity would not affect the transport properties in all the investigated polymer fluids (Figures 5B, 9). Conversely, shear-induced depletion was affected by the significant decrease of V in the PVP 360 concentration range we tested, where our results on motility are consistent with previous findings. Despite the drastic reduction of cell motility with increasing concentration of PVP360, we observe that the increase in transit time t_{run} still makes it possible to experimentally observe depletion at a distance $D = 50$ cm from the inlet of the channel even for the 10 w/v% solution. In the non-Newtonian case, the xanthan gum solution used in our study did not induce an enhancement of the swimming velocity observed, for example, for *E. coli* in Methocel [11] and in carboxy-methyl cellulose [12], but not for *V. cholerae* in mucin [7]. Given the complex interplay between flagellar motility and rheology of polymer fluids [11, 19], the differences in the observations could be attributed to the particular bacterium and polymer we chose.

The mathematical model accounts for the change in viscosity and bacterial motility of the different solutions. However, it does not account for the microscopic structure of the polymeric fluids, the possible structural changes caused by the shear flow, and the consequent impact they would have on bacterial motility. The discrepancies between the concentration profiles B obtained with the experiments and the numerical simulations at high shear rates and high concentrations in PVP 360 and at high shear rates in the xanthan gum solution could be explained in light of the shear-induced structural rearrangements of the suspending fluid at the microscale. In these cases, the bulk rheological behavior may not be sufficient to fully capture the complex interplay between bacterial motility and the polymeric fluid structure described in [11, 19]. However, our simplified model was able to describe the overall trend of the shear-induced depletion, indicating that the rheology of the fluid and a realistic description of the bacterial swimming pattern are the most important factors driving bacterial transport in flow.

Interestingly, although the viscosity of PVP 360 5 w/v% ($\eta = 38$ mPa s, Figure 1B) is significantly lower than the zero-shear viscosity of the xanthan gum solution ($\eta_0 = 160$ mPa s, Figure 1C), the shear-induced depletion was consistently lower in the Newtonian PVP 360 case. In the non-Newtonian case, the similarity between the experimental and the numerical B profiles obtained at constant bacterial swimming velocity ($V_{0.1\%}$ and $V(\eta_s)$) suggests that two main factors contribute to the strong depletion observed in the non-Newtonian case: the high value of the bacterial swimming velocity V (Figure 6A) and the non-Newtonian shear rate profile $\dot{\gamma}$ (Figure 7). In xanthan gum 0.1 w/v% solution, $V_{0.1\%}$ is reduced by only 15% with respect to the buffer, while in PVP 360 5 w/v%, the reduction is of about 80%, even if the η_0 of xanthan gum 0.1 w/v% is 4 times higher than the viscosity of PVP 360 5 w/v%. The high value of V in the xanthan gum solution could be attributed to the local shear-thinning performed by the bacterial flagella. Moreover, since the concentration profiles B obtained by simulations at constant V are in good agreement with the experiments, at least at low

average shear rates S , we hypothesize that the local shear-thinning induced by the bacterial swimming is not deeply affected by the local flow conditions. The slight increase in B at the centerline of the channel—resulting from the numerical simulation at $V(y)$ —is not observed in the experiments. Since the variation of $\eta(y)$ in the channel is appreciable over few tens of microns, this length scale may be too similar to the length of a bacterium (including the flagellum) to appreciably affect the bacterial swimming speed. At higher shear rates, more complex interactions between flagella and the fluid or changes in the fluid structure [11] may lead to the observed discrepancies.

Given the impact of shear-induced depletion on surface colonization [23, 29] and bacterial chemotaxis [23, 26], our findings could have substantial medical and technological implications. For example, the respiratory, gastrointestinal, and reproductive tracts of animals are covered in mucus [1], a complex polymer fluid which is continuously stirred by ciliary motion. In these systems, a realistic description of bacterial transport and surface colonization would require to take into account the interplay between shear rate, cell motility and fluid rheology. By describing two prototypical cases, we hope to raise the interest of the community and foster further investigation in more complex scenarios, contributing to the creation of a more accurate description of bacterial transport in polymer solutions.

DATA AVAILABILITY STATEMENT

The original contributions presented in the study are included in the article/Supplementary Material, further inquiries can be directed to the corresponding author.

AUTHOR CONTRIBUTIONS

ES, RR, and RS designed research. GS, ES, TC, and YL performed the experiments. GS and ES analysed all the data. SG performed the rheological characterization of the polymer solutions. GS, ES, and RR designed and built the mathematical model. GS and ES wrote the manuscript and all authors edited and commented on the manuscript.

FUNDING

The authors acknowledge support from SNSF PRIMA grant 179834 (to ES), from a Symbiosis in Aquatic Systems Investigator Award from the Gordon and Betty Moore Foundation (GBMF9197; <https://doi.org/10.37807/GBMF9197>) (to RS), and from Simons Foundation Grant 542395 (to RS) as part of the Principles of Microbial Ecosystems Collaborative (PriME). Open access funding provided by ETH Zurich.

ACKNOWLEDGMENTS

The authors acknowledge Dr. Sam Charlton and Ursin Eberhard for the insightful discussions; Ela Burmeister for the technical support.

REFERENCES

- Lai SK, Wang Y-Y, Wirtz D, Hanes J. Micro- and Macrorheology of Mucus. *Adv Drug Deliv Rev* (2009) 61:86–100. doi:10.1016/j.addr.2008.09.012
- Morgan SE, McCormick CL. Water-soluble Polymers in Enhanced Oil Recovery. *Prog Polym Sci* (1990) 15:103–45. doi:10.1016/0079-6700(90)90017-U
- Sunthar P. Polymer Rheology. In: JM Krishnan, AP Deshpande, PBS Kumar, editors. *Rheology of Complex Fluids*. New York, NY: Springer (2010). p. 171–91. doi:10.1007/978-1-4419-6494-6_8
- Schneider WR, Doetsch RN. Effect of Viscosity on Bacterial Motility. *J Bacteriol* (1974) 117:696–701. doi:10.1128/jb.117.2.696-701.1974
- Berg HC, Turner L. Movement of Microorganisms in Viscous Environments. *Nature* (1979) 278:349–51. doi:10.1038/278349a0
- Kaiser GE, Doetsch RN. Enhanced Translational Motion of *Leptospira* in Viscous Environments. *Nature* (1975) 255:656–7. doi:10.1038/255656a0
- Grognot M, Mittal A, Taute KM. *Vibrio cholerae* Motility in Aquatic and Mucus-Mimicking. *Appl Environ Microbiol* (2021) 87:e01293–21. doi:10.1128/aem.01293-21
- Keller JB. Effect of Viscosity on Swimming Velocity of Bacteria. *Proc Natl Acad Sci U.S.A* (1974) 71:3253–4. doi:10.1073/pnas.71.8.3253
- Magariyama Y, Kudo S. A Mathematical Explanation of an Increase in Bacterial Swimming Speed with Viscosity in Linear-Polymer Solutions. *Biophysical J* (2002) 83:733–9. doi:10.1016/S0006-3495(02)75204-1
- Martinez VA, Schwarz-Linek J, Reufer M, Wilson LG, Morozov AN, Poon WCK. Flagellated Bacterial Motility in Polymer Solutions. *Proc Natl Acad Sci U.S.A* (2014) 111:17771–6. doi:10.1073/pnas.1415460111
- Qu Z, Breuer KS. Effects of Shear-Thinning Viscosity and Viscoelastic Stresses on Flagellated Bacteria Motility. *Phys Rev Fluids* (2020) 5:1–14. doi:10.1103/PhysRevFluids.5.073103
- Patteson AE, Gopinath A, Goulian M, Arratia PE. Running and Tumbling with *E. coli* in Polymeric Solutions. *Sci Rep* (2015) 5:1–11. doi:10.1038/srep15761
- Li C, Qin B, Gopinath A, Arratia PE, Thomases B, Guy RD. Flagellar Swimming in Viscoelastic Fluids: Role of Fluid Elastic Stress Revealed by Simulations Based on Experimental Data. *J R Soc Interf* (2017) 14:20170289. doi:10.1098/rsif.2017.0289
- Qin B, Gopinath A, Yang J, Gollub JP, Arratia PE. Flagellar Kinematics and Swimming of Algal Cells in Viscoelastic Fluids. *Sci Rep* (2015) 5:9190. doi:10.1038/srep09190
- Kamdar S, Shin S, Leishangthem P, Francis LF, Xu X, Cheng X. The Colloidal Nature of Complex Fluids Enhances Bacterial Motility. *Nature* (2022) 603:819–23. doi:10.1038/s41586-022-04509-3
- Liu B, Powers TR, Breuer KS. Force-free Swimming of a Model Helical Flagellum in Viscoelastic Fluids. *Proc Natl Acad Sci U.S.A* (2011) 108:19516–20. doi:10.1073/pnas.1113082108
- Spagnolie SE, Liu B, Powers TR. Locomotion of Helical Bodies in Viscoelastic Fluids: Enhanced Swimming at Large Helical Amplitudes. *Phys Rev Lett* (2013) 111:1–5. doi:10.1103/PhysRevLett.111.068101
- Qu Z, Temel FZ, Henderix R, Breuer KS. Changes in the Flagellar Bundling Time Account for Variations in Swimming Behavior of Flagellated Bacteria in Viscous media. *Proc Natl Acad Sci U.S.A* (2018) 115:1707–12. doi:10.1073/pnas.1714187115
- Zöttl A, Yeomans JM. Enhanced Bacterial Swimming Speeds in Macromolecular Polymer Solutions. *Nat Phys* (2019) 15:554–8. doi:10.1038/s41567-019-0454-3
- Wheeler JD, Secchi E, Rusconi R, Stocker R. Not just Going with the Flow: The Effects of Fluid Flow on Bacteria and Plankton. *Annu Rev Cel Dev. Biol.* (2019) 35:213–37. doi:10.1146/annurev-celldbio-100818-125119
- Rusconi R, Stocker R. Microbes in Flow. *Curr Opin Microbiol* (2015) 25:1–8. doi:10.1016/j.mib.2015.03.003
- Son K, Brumley DR, Stocker R. Live from under the Lens: Exploring Microbial Motility with Dynamic Imaging and Microfluidics. *Nat Rev Microbiol* (2015) 13:761–75. doi:10.1038/nrmicro3567
- Rusconi R, Guasto JS, Stocker R. Bacterial Transport Suppressed by Fluid Shear. *Nat Phys* (2014) 10:212–7. doi:10.1038/NPHYS2883
- Ezhilan B, Saintillan D. Transport of a Dilute Active Suspension in Pressure-Driven Channel Flow. *J Fluid Mech* (2015) 777:482–522. doi:10.1017/jfm.2015.372
- Stark H. Swimming in External fields. *Eur Phys J Spec Top* (2016) 225:2369–87. doi:10.1140/epjst/e2016-60060-2
- Bearon RN, Hazel AL. The Trapping in High-Shear Regions of Slender Bacteria Undergoing Chemotaxis in a Channel. *J Fluid Mech* (2015) 771:1–13. doi:10.1017/jfm.2015.198
- Miño GL, Baabour M, Chertcoff R, Gutkind G, Clément E, Auradou H, et al. *E. coli* Accumulation behind an Obstacle. *AiM* (2018) 08:451–64. doi:10.4236/aim.2018.86030
- Altshuler E, Miño G, Pérez-Penichet C, Río Ld., Lindner A, Rousselet A, et al. Flow-controlled Densification and Anomalous Dispersion of *E. coli* through a Constriction. *Soft Matter* (2013) 9:1864–70. doi:10.1039/c2sm26460a
- Secchi E, Vitale A, Miño GL, Kantsler V, Eberl L, Rusconi R, et al. The Effect of Flow on Swimming Bacteria Controls the Initial Colonization of Curved Surfaces. *Nat Commun* (2020) 11:2851. doi:10.1038/s41467-020-16620-y
- Ślomska J, Alcolombri U, Secchi E, Stocker R, Fernandez VI. Encounter Rates between Bacteria and Small Sinking Particles. *New J Phys* (2020) 22:043016. doi:10.1088/1367-2630/ab73c9
- Mcdonald JC, Duffy DC, Anderson JR, Chiu DT, Wu H, Schueller OJA, et al. Fabrication of Microfluidic Systems in Poly(dimethylsiloxane). *Electrophoresis* (2000) 21:27–40. doi:10.1002/(sici)1522-2683(20000101)21:1<27::aid-elps27>3.0.co;2-c
- Wyatt NB, Liberatore MW. Rheology and Viscosity Scaling of the Polyelectrolyte Xanthan Gum. *J Appl Polym Sci* (2009) 114:4076–84. doi:10.1002/app.31093
- Cai Q, Li Z, Ouyang Q, Luo C, Gordon VD. Singly Flagellated *Pseudomonas aeruginosa* Chemotaxes Efficiently by Unbiased Motor Regulation. *MBio* (2016) 7:7. doi:10.1128/mBio.00013-16
- Qian C, Wong CC, Swarup S, Chiam K-H. Bacterial Tethering Analysis Reveals a "Run-Reverse-Turn" Mechanism for *Pseudomonas* Species Motility. *Appl Environ Microbiol* (2013) 79:4734–43. doi:10.1128/AEM.01027-13
- Taylor BL, Koshland DE. Reversal of Flagellar Rotation in Monotrichous and Peritrichous Bacteria: Generation of Changes in Direction. *J Bacteriol* (1974) 119:640–2. doi:10.1128/jb.119.2.640-642.1974

Conflict of Interest: The authors declare that the research was conducted in the absence of any commercial or financial relationships that could be construed as a potential conflict of interest.

Publisher's Note: All claims expressed in this article are solely those of the authors and do not necessarily represent those of their affiliated organizations, or those of the publisher, the editors and the reviewers. Any product that may be evaluated in this article, or claim that may be made by its manufacturer, is not guaranteed or endorsed by the publisher.

Copyright © 2022 Savorana, Geisel, Cen, Ling, Stocker, Rusconi and Secchi. This is an open-access article distributed under the terms of the Creative Commons Attribution License (CC BY). The use, distribution or reproduction in other forums is permitted, provided the original author(s) and the copyright owner(s) are credited and that the original publication in this journal is cited, in accordance with accepted academic practice. No use, distribution or reproduction is permitted which does not comply with these terms.